JOURNAL OF APPLIED PHYSICS 110, 043517 (2011)

Temperature dependence of surface phonon polaritons from a quartz grating

Andrew K. Hafeli,[1,a] Eden Rephaeli,[2] Shanhui Fan,[2] David G. Cahill,[1] and Thomas E. Tiwald[3]
[1]*Department of Materials Science and Engineering, Materials Research Laboratory, University of Illinois at Urbana-Champaign, Urbana, Illinois 61801, USA*
[2]*Department of Electrical Engineering, Ginzton Laboratory, Stanford University, Stanford, California 94305, USA*
[3]*J.A. Woollam Corporation, 645 M St., Suite 102, Lincoln, Nebraska 68508, USA*

(Received 6 January 2011; accepted 4 July 2011; published online 23 August 2011; corrected 31 August 2011)

We report the temperature dependence of the surface phonon polariton (SPhP) spectra of α-SiO_2 (quartz), propagated to the far-field by a grating, in the temperature range between 300 K and 800 K. Room temperature data for a 670 nm deep grating are compared to a simulated spectrum using a finite-difference frequency-domain approach. The inputs to the simulation are the dielectric functions measured by infrared ellipsometry and modeled as a set of damped oscillators. The simulated spectra are in good agreement with experiment. The width of the SPhP reflectivity dip depends on the depth of the grating. For a grating depth of 280 nm, the width of the reflectivity dip in the temperature range $300 < T < 800$ K is comparable to what is expected for the SPhP excitations of a flat surface. For a grating depth of 670 nm, the width of the reflectivity dip increases significantly due to coupling to far-field radiation. © *2011 American Institute of Physics*. [doi:10.1063/1.3624603]

INTRODUCTION

Surface phonon polaritons (SPhP) are coupled modes of electromagnetic waves and optical phonons confined to the interface between a polar material and a lossless dielectric. SPhP have been used to create narrow bandwidth directional thermal emission,[1–4] enhance radiative heat transport in the near-field,[5] and, most recently, rectify radiative thermal transport.[6] In Ref. 6, Otey and co-workers showed that rectification of thermal transport by near-field radiation can be achieved through temperature dependent changes of the SPhP spectrum.[6] The two sides of the thermal diode were chosen to have distinct but closely spaced peaks in the density of states of the SPhP. Because the position of the peak shifts with temperature, heating of one side of the diode increases the overlap of the SPhP peaks of the two materials while heating the other side of the diode causes the overlap to decrease. Rectification is strongest if the shift in the position of the peak in the density of states is comparable to the bandwidth of the SPhP.

Therefore, a key parameter of a thermal diode based on near-field radiation is the bandwidth Γ of the SPhP; Γ is connected to the damping of the optical phonon through the complex dielectric constant.[5,7] The damping of the optical phonon typically increases as the temperature increases due to anharmonicity.[8] Therefore, as the temperature increases, we can expect Γ will increase.

For flat surfaces, the width of the SPhP modes increases monotonically from 30% of the phonon damping at the transverse phonon frequency to the intrinsic phonon damping at ω_s.[9] In our experiments, we use a grating to couple the SPhP to far-field radiation. Intrinsic scattering by the grating profile and extrinsic scattering by surface roughness are thought to increase the width of the SPhP peaks[10] although an exact expression for the width is not known.

The materials studied in Ref. 6 were two polytypes of SiC. In our current work, we have chosen to study experimentally and theoretically a prototypical oxide crystal, α-SiO_2 (quartz). Quartz crystals are commercially available at low cost. The optical phonon frequencies are relatively high, comparable to those of SiC. SPhP excitations of quartz have been previously studied at room temperature.[11–14] We use an etched grating to couple the SPhP to the far-field and study the SPhP spectra using measurements of infrared reflectivity.

Quartz has trigonal symmetry at room temperature that gives rise to anisotropy in the dielectric constant with the extraordinary direction along the c-axis and the ordinary direction in the a-b plane.[15] At 573 °C, quartz transforms from the α to the β phase; the crystal structure changes from trigonal to hexagonal. The change in phonon damping with temperature has been shown to increase significantly near the phase transition.[16] Abrupt changes in the optical phonon spectra at phase transformations may provide another mechanism for creating additional functional control of radiative thermal transport.

EXPERIMENTAL DETAILS

We etched gratings into 1 mm thick plate-shaped crystals of Z-cut α-quartz. (Z-cut denotes a crystallographic orientation of α-quartz with the c-axis perpendicular to the surface.) A 100 nm film of Cr was sputtered on the quartz sheets as an etch mask. Standard photolithographic procedures were used to pattern the Cr mask into an array of lines over a 1×1 cm^2 area. The quartz was then wet etched using

[a]Author to whom correspondence should be addressed. Electronic mail: hafeli1@illinois.edu.

 © 2011 American Institute of Physics

an etchant concentration of 2:3 hydrofluoric acid (49% conc.) to ammonium fluoride (39.5% conc.) at 55 °C to minimize roughness.[17,18] The grating periodic direction was always aligned with the *a*-axis, or X-direction, to maximize the difference between the lateral (2 μm/h) and vertical (25 μm/h) etch rates; the high anisotropy of the etch rates, should, in principle, enable nearly vertical side walls. The sidewall profile was measured using cross-section scanning electron microscopy. On one side of the channel, the sidewall was within 5 degrees of vertical; on the other side of the channel, the profile of the side-wall has a 45° facet that extends $\sim$350 nm from the sidewall in the 670 nm depth sample.

A period of 7 μm was chosen so that we could probe the dispersion of the SPhP, i.e., the angle dependent frequency, at experimentally accessible angles. Simulations of the reflectivity spectrum at room temperature were used to select the depth of the grating and maximize the dip in reflectivity of the lowest frequency SPhP feature. Following the approach of Ref. 1, one third of the grating spacing is etched and the remainder is unetched. Depth and roughness were measured by atomic force microscopy, see Fig. 1. The depth measured by AFM is 670 ± 10 nm over the full area of the grating. The roughness of etched and unetched surfaces was 2.9 nm rms and 2.6 nm rms, respectively, measured over areas of 2×30 μm^2. We fabricated and studied a second grating with a depth of 280 nm to reveal the effects of far-field radiative coupling on the damping of the SPhP.

We used measurements of angle-resolved infrared reflectivity to determine the SPhP spectrum of the quartz grating. A 10 W globar source was mounted on the rotating arm of a θ-2θ stage and the blackbody radiation was collected and made into a parallel beam by a parabolic collecting mirror with a 5 cm focal length and an f# of 2. After reflection from the sample, the infrared light passes through an aperture that controls the region of the sample that is probed by the spectrometer, $\sim$5 mm in diameter and focused at the input of a Fourier transform infrared (FTIR) spectrometer by a parabolic mirror. The resolution of the spectrometer was 2 cm^{-1}. Since only radiation with the electric field oriented in the plane of incidence (Transverse magnetic- polarized) couples to the SPhP, a CaF wire grid polarizer with an extinction ratio of 300:1 was used to filter the reflected light. Samples were mounted so that the grating periodic direction (*a*-axis) and the electric field were both in the plane of incidence. The reflectivity of a Ag film, which has a reflectivity of greater than 98% in the spectral region of interest, was used as a standard.

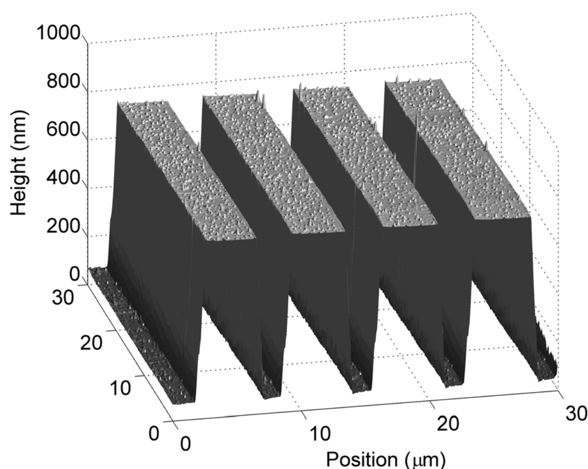

FIG. 1. AFM image of the quartz grating structure with periodicity 7 μm and depth 670 nm.

Because the frequency of the SPhP mode that we are most interested in depends strongly on angle, uncertainties in the angles are a concern. The angular accuracy of the stage is $\approx$1°, determined by the accuracy of the angle markings on the stages. The spread in angles of light illuminating the sample was larger than the spread in angles accepted by the collecting optics. The angular acceptance from the samples were limited by the numerical aperture of the mirror that focuses the light into the spectrometer, which was calculated to be approximately $\pm 1°$ based on spot size 5 mm and focal length of 153 mm.

The samples were mounted on a temperature-controlled stage capable of reaching 800 K. The temperature was measured by a Pt resistance thermometer mounted directly on the sample. The temperature of the sample varied by $\pm$ 2 K during each measurement due to limitations of the temperature controller. The accuracy stated by the manufacturer of the Pt resistance thermometer varies from $\pm$ 0.3 K at 273 K to $\pm$ 2.8 K at 773 K. We estimate that the overall accuracy of the temperature is within $\pm$ 10 K. When the sample is at elevated temperatures, it emits a significant amount of infrared light. This background signal was measured with the spectrometer source blocked off and then subtracted from the infrared reflectivity data.

Ellipsometry measurements were performed on flat and unpatterned Z-cut and X-cut quartz using a J.A. Woollam IR-VASE spectroscopic ellipsometer in the spectral range of 300 cm^{-1} to 4000 cm^{-1}. The ellipsometery data has a resolution of 2 cm^{-1}.

Two sets of data were collected for X-cut quartz: (i) with the optic axis parallel to the plane of incidence (POI) and (ii) with the optic axis perpendicular to the POI. Two measurements are required because a single ellipsometric measurement provides only two quantities (Ψ and Δ) at every wavelength and four independent quantities are needed to specify two complex dielectric functions. The two measurements must also be independent. This is easy to accomplish with X-cut quartz because the optic axis is parallel to the surface and the ordinary and extraordinary dielectric response can be excited by varying degrees by rotating the sample with respect to the POI.

The complexity of the data acquisition and analysis is substantially reduced by choosing the optic axis parallel to the POI for one measurement and perpendicular to the POI for the second measurement. At these orientations the electric field components are aligned with the principle optical directions, which allows one to acquire standard ellipsometric data, i.e., the complex ratio of the diagonal Fresnel coefficients.[19]

The two data sets were simultaneously fit to two uniaxial models. Each model defined a different orientation of the optic axis, but both models shared the same ordinary and extraordinary dielectric functions defined by a summation of

TABLE I. Oscillator model parameters from ellipsometry measurements.

	Ordinary				Extraordinary		
n	An	En (cm^{-1})	Br (cm^{-1})	n	An	En (cm^{-1})	Br (cm^{-1})
1	44.021	393.61	3.3	1	68.024	363.93	3.6
2	101.700	449.84	3.7	2	0.212	415.64	15.5
3	1.906	694.89	8.3	3	82.130	494.17	4.5
4	12.722	794.88	7.5	4	12.639	776.03	7.2
5	105.396	1065.23	6.9	5	120.713	1073.38	6.3
6	0.016	1142.33	3.6	6	0.040	1189.25	16.1
7	1.258	1160.85	8.0	7	0.027	1237.95	54.5
8	0.048	1175.36	176.8	8	0.052	1275.09	120.1
9	0.038	1270.83	39.4	9	0.042	1609.97	35.4
10	0.041	1875.00	34.7	10	0.026	1688.31	24.6
				11	0.012	1791.12	26.2
				12	0.053	1876.05	43.6
	ε_∞	2.3839			ε_∞	2.412	

oscillators, see Eq. (1). A computer-controlled numerical regression analysis[20] simultaneously varied the oscillator parameters of both dielectric functions until generated data fit experimental data from both orientations. The Z-cut sample (optic axis oriented perpendicular to the surface) was also measured, and the data were plotted against the results from the X-cut data analysis as a consistency check.

Phonon damping is included in the dielectric constant of the oscillator model fit of the ellipsometry data

$$\varepsilon(E) = \varepsilon_\infty + \sum_{n=1}^{n_{\max}} \frac{A_n Br_n E_n}{E_n^2 - E^2 - iBr_n E}, \tag{1}$$

where Br_n is the phonon damping of the nth mode, E_n are the phonon frequencies, and A_n are the amplitudes. These parameters are listed in Table I. Several investigators have made similar models for quartz from reflectivity and ellipsometry, but a more detailed analysis of the frequency range we are interested in is needed for more accurate modeling.[15,16,21,22] There are many extra oscillators in this model that do not correspond to actual phonons, but are used to make a more accurate fit of the ellipsometry data.

Simulations of the reflectivity spectra of the 670 nm deep grating were performed using a 2D finite-difference frequency-domain code, in which Maxwell's equations for TM-polarized light (H-field transverse to the plane of incidence) were discretized and solved, one frequency at a time.[23] Bloch boundary conditions were enforced in the transverse direction. The total size of the computational cell was fixed at 7 μm by 20 μm, with a grid point resolution of 70 nm by 10 nm in the transverse and longitudinal direction, respectively. A perfectly matched layer (PML) was implemented in the longitudinal direction to avoid spurious reflections at the edge of the computational cell.[24] A thin slab was added below the grating and truncated inside the PML region to simulate an infinitely thick substrate. The simulation used both the ordinary ray and extraordinary ray dielectric constant measured by ellipsometry to accurately model the biaxial nature of the material.

RESULTS AND DISCUSSION

The dispersion relation for SPhP can be derived by solving Maxwell's equations at the interface between two materials.[9,10,25,26] When the first material is anisotropic and the second material is air, the expression simplifies to

$$K_{//} = \frac{\omega}{c}\left(\frac{\varepsilon_{//}\varepsilon_\perp - \varepsilon_{//}}{\varepsilon_{//}\varepsilon_\perp - 1}\right)^{\frac{1}{2}}, \tag{2}$$

where $\varepsilon_{//}$ is the dielectric constant parallel to the optic axis (extraordinary direction) and the $\varepsilon_\perp$ is the dielectric constant perpendicular to the optic axis (ordinary direction).

The ordinary direction is the direction of surface wave propagation along the interface.[13,27] This dispersion relation also describes the brewster modes that are above the light line and are propagating modes.[28] From Eq. (2) it can be seen that the SPhP is at resonance when $\varepsilon_{//}\varepsilon_\perp = 1$ where both dielectric constants are negative, which is known as the SPhP frequency ω_s.

By etching a grating into the surface, the dispersion relation is modified by the grating and wavevectors outside of the first Brillouin zone are translated into it by a multiple of $\frac{2\pi}{d}$,[29]

$$\frac{2\pi}{\lambda}\sin(\theta) = K_{//} - p\left(\frac{2\pi}{d}\right). \tag{3}$$

In Eq. (3), θ is the angle of incidence, λ is the incident wavelength, and d is the grating periodicity. The grating then provides the large wavenumber SPhP modes a momentum "kick", which enables them to couple to free propagating modes of the electromagnetic far-field.

The dispersion relation is further modified by the finite depth of the grating. The combination of Eqs. (2) and (3) yields the dispersion relation of a flat surface, but with a periodic surface profile, band gaps between the transverse phonon frequency and the SPhP frequency open up and grow with increasing depth. We observed in our simulations that the strengths of scattering of different frequency SPhPs also depend on depth, in agreement with previous work.[30] For example, the dips in the reflectivity spectrum at 1100 cm^{-1} and 1207 cm^{-1} are maximized for grating depths of 670 nm and 1200 nm, respectively.

Figure 2(a) shows simulated and measured reflectivity spectra of a quartz 670 nm depth grating at 8° from normal incidence. Data for a flat quartz surface are included for comparison. Features in the spectra correspond to the bands in the dispersion relation of SPhPs. According to Eq. (3), varying the angle allows us to vary the wavevector parallel to the surface and probe a segment of the dispersion relation. For each angle or wavevector, the frequencies of the dips in reflectivity are recorded and the dispersion relation is obtained. The frequency of the dip near 1100 cm^{-1} is different between the simulated and measured spectrum but this difference is within the experimental uncertainties created by the uncertainties in the angle of incidence.

Figure 2(b) shows the change in the reflectivity spectra with temperature. As the temperature increases, we observe several changes in the spectra, including the broadening of the SPhP

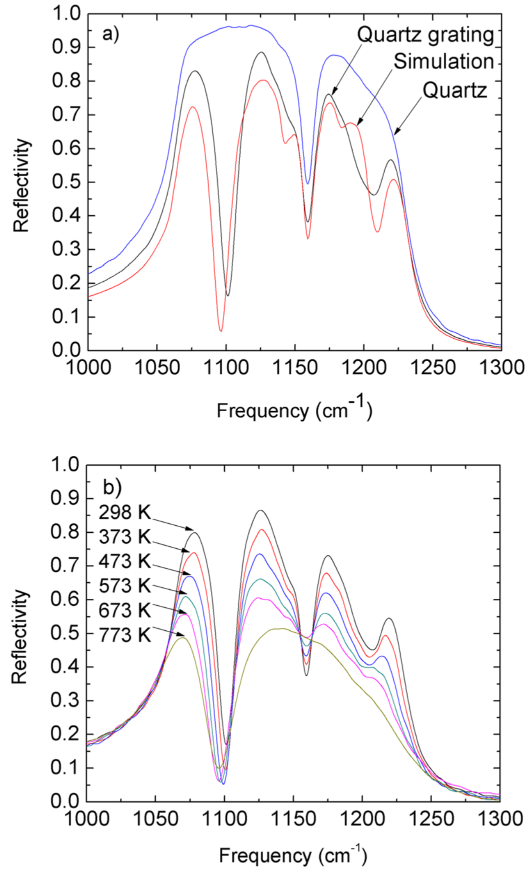

FIG. 2. (Color online) (a) Reflectivity spectra of quartz with and without a grating plotted with the simulated quartz grating spectra. (b) Changes in the quartz grating reflectivity spectra with temperature.

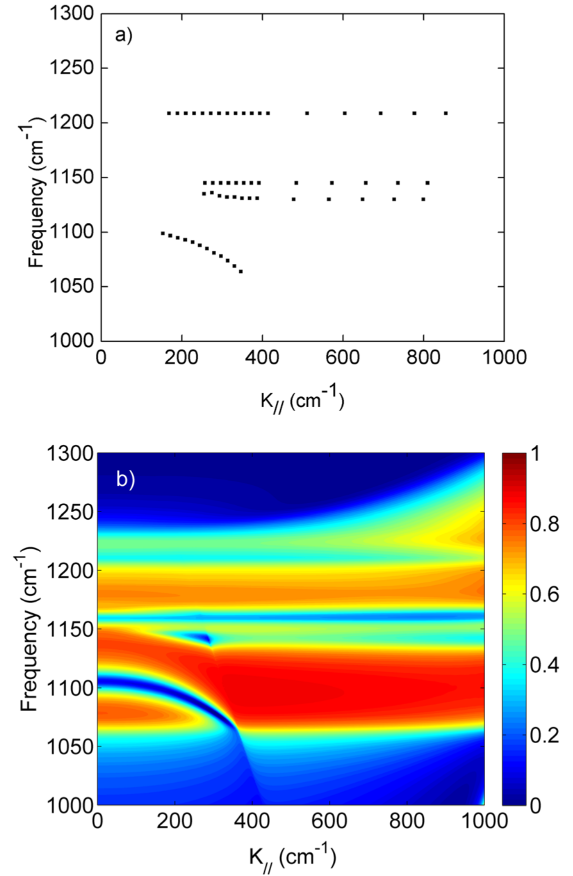

FIG. 3. (Color online) (a) Dispersion relation from experiment and (b) simulated reflectivity. Experimentally, varying the in-plane wavevector corresponds to varying the angle of incidence, see Eq. (3). Each point corresponds to the frequency of a dip in reflectivity and the corresponding angle converted to wavevector. In (b), the color scale shows reflectivity from 0 to 1. The low reflectivity lines correspond to SPhP branches.

features and the broadening of the transverse optical phonon dip at 1161 cm^{-1}. At 773 K, the broadening is highly pronounced.

Figure 3 compares the experimentally measured dispersion relation of a 670 nm depth grating at room temperature with the simulated reflectivity spectrum. The two are quite similar as the existence of SPhP modes translates into low reflectivity. The SPhP frequency obtained from the dielectric constant condition $\varepsilon_{//}\varepsilon_{\perp} = 1$ is $\omega_s = 1185$ cm^{-1}, which corresponds to the highest frequency band of the dispersion relation. The ordinary direction transverse phonon at 1161 cm^{-1} approaches this condition and shifts the dispersion to higher $K_{//}$ near this frequency. Measured and simulated values for the highest band appear at a higher frequency, 1210 cm^{-1} and 1207 cm^{-1}, respectively, than the predicted ω_s due to the shift of the dispersion relation created by the finite depth of the grating. The highest band of the 280 nm sample was too weak to measure.

The full-width-at-half-maximum (FWHM) for the SPhP dip near 1100 cm^{-1} was measured every 25 K between room temperature and 800 K. The temperature dependent measurements were performed at 8° from the surface normal for the 670 nm deep grating and 12° for the 280 nm deep grating to place the SPhP dip at 1100 cm^{-1}, a frequency where the FWHM can be measured accurately.

The FWHM of the reflectivity dip at 1100 cm^{-1} was determined by a non-linear least squares fit of the spectra to a sum of Lorentzians. Figure 4 shows that the changes in the FWHM of the SPhP feature for both gratings have the same temperature dependence. The FWHM of the deeper grating is offset from the FWHM of the shallower grating by a constant, $\approx$ 10 cm^{-1}. The FWHM of the reflectivity dip is a measure of the damping of the SPhP. The damping of the SPhP is controlled by the lifetime of the optical phonon due to anharmonic interactions with other phonons and coupling of the SPhP to far-field electromagnetic radiation.

We now compare the damping we observe in our experiments to the SPhP damping predicted for a flat surface based on the damping of the transverse optical phonon (Γ_{TO}).[9]

$$\Gamma(\omega) = \frac{\frac{1}{2}\omega\frac{\partial\varepsilon(\omega)}{\partial\omega}\Gamma_{TO}}{\varepsilon(\omega)(1+\varepsilon(\omega)) + \frac{1}{2}\omega\frac{\partial\varepsilon(\omega)}{\partial\omega}}, \tag{4}$$

where $\Gamma(\omega)$ is the predicted damping for a flat surface. Values for the damping of the transverse optical phonon at elevated temperature Γ_{TO} were obtained from the literature.[16] Equation (4) was evaluated using the dielectric constant obtained from ellipsometric measurements at room temperature. The change in $\Gamma(\omega)$ with temperature is primarily due to the change in Γ_{TO} since the remainder of the equation

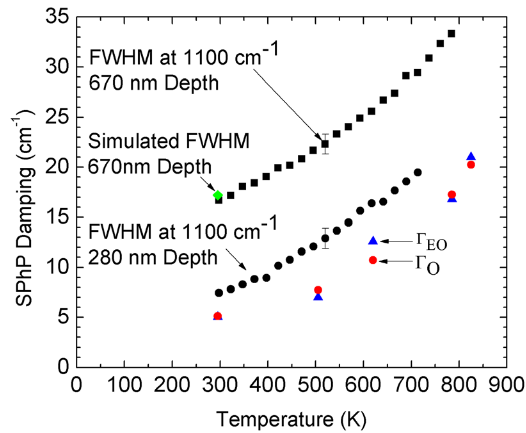

FIG. 4. (Color online) Temperature dependence of the FWHM of the dip in reflectivity at 1100 cm^{-1} for two grating depths plotted with the flat SPhP damping for the ordinary (Γ_O) and extraordinary (Γ_{EO}) transverse phonons. Changes in FWHM correspond to changes in the phonon damping. The simulated FWHM at 1100 cm^{-1} is also plotted and is similar to the experimental value at room temperature. Error bars representative of all measured data points can be found on one temperature data point for each grating depth.

changes by less than 5% between 300 and 800 K. The transverse optical phonons of interest have room- temperature frequencies of 1073 cm^{-1} and 1065 cm^{-1} for the extra-ordinary and the ordinary direction, respectively. The room temperature damping for these phonons is 6.8 and 7.2 cm^{-1}, and from Eq. (4) the damping of the SPhP of a flat surface is predicted to be 70% and 75% of these values, respectively. The elevated temperature damping parameters from Ref. 16 were converted to SPhP damping for the flat surface condition and plotted along with the FWHM of the feature at 1100 cm^{-1}. (Measurements of reflectivity at elevated temperature could have been used to obtain the phonon dampings but we felt we could not substantially improve upon the data in Ref. 16.) The damping is approximately 12 cm^{-1} higher than that of a flat surface; we attribute this additional temperature independent damping to damping created by coupling to far-field radiation induced by the grating.[10] FWHM data for the 280 nm deep grating are closer to the predicted damping, as expected. The excellent agreement between the simulated and measured values of the FWHM of the 670 nm grating help us rule out a significant role of random surface roughness or other material condition effects on the damping of the SPhP.

The 670 nm deep grating exhibits near-zero reflectivity at the resonance frequencies. Thus, we can infer that we are close to critical coupling condition, characterized by a radiative coupling rate (due to the grating) equal to the "flat surface" SPhP loss rate as can be inferred by the linewidth of surface phonon polartion on a flat-surface.[31] Thus, in this case the total damping rate, combining both the radiative coupling rate due to the grating and the material absorption rate, is approximately twice the "flat surface" SPhP loss rate, consistent with the data shown in Fig. 4.

CONCLUSION

In conclusion, the FWHM of the SPhP features coupled to the far-field by a grating increase with increasing temperature, corresponding to an increase in the bulk transverse phonon damping. The simulated spectra and dispersion relation agree well with the reflectivity data at room temperature. The agreement between experiment and simulation at room temperature shows that the grating produces an increase of the damping of the SPhP over what is expected for a flat surface, in agreement with coupled-mode theory.[31]

ACKNOWLEDGMENT

This work was supported by the US Air Force Office of Scientific Research Grant No. MURI FA9550-08-1-0407.

[1]J. Greffet, R. Carminati, K. Joulain, J. Mulet, S. Mainguy, and Y. Chen, Nature **416**, 6876 (2002).
[2]B. J. Lee and Z. M. Zhang, J. Heat Transfer **129**, 1 (2007).
[3]P. Ben-Abdallah, J. Opt. Soc. Am. A **21**, 7 (2004).
[4]M. Laroche, C. Arnold, F. Marquier, R. Carminati, J. Greffet, S. Collin, N. Bardou, and J. Pelouard, Opt. Lett.**30**, 19 (2005).
[5]J. Mulet, K. Joulain, R. Carminati, and J. Greffet, Microscale Thermophys. Engin. **6**, 3 (2002).
[6]C. Otey, W. T. Lau, and S. Fan, Phys. Rev. Lett. **104**, 15 (2010).
[7]S. Basu and Z. M. Zhang, J. Appl. Phys. **105**, 9 (2009).
[8]R. A. Cowley, Rep. Prog. Phys. **31**, 1 (1968).
[9]J. Nkoma, R. Loudon, and D. R. Tilley, J. Phys. C **7**, 19 (1974).
[10]D. L. Mills and V. M. Agranovich, *Surface Polaritons: Electromagnetic Waves at Surfaces and Interfaces* (North-Holland/Elsevier Science, New York, 1982), p. 717.
[11]G. N. Zhizhin, V. I. Silin, V. A. Sychugov, and V. A. Yakovlev, Solid State Commun. **51**, 8 (1984).
[12]K. T. Antonova, S. A. Voronov, V. A. Yakovlev, and G. N. Zhizhin, Opt. Commun. **60**, 4 (1986).
[13]H. J. Falge and A. Otto, Phys. Status Solidi B **66**, 523 (1973).
[14]E. Schuller, G. Borstel, and H. J. Falge, Physica Status Solidi B **69**, 2 (1975).
[15]W. G. Spitzer and D. A. Kleinman, Phys. Rev. **121**, 5 (1961).
[16]F. Gervais and B. Piriou, Phys. Rev. B **11**, 10 (1975).
[17]C. Hedlund, U. Lindberg, U. Bucht, and J. Soderkvist, J Micromech. Microeng. **3**, 2 (1993).
[18]P. Rangsten, C. Hedlund, I. V. Katardjiev, and Y. Bäcklund, J. Micromech. Microeng. **8**, 1 (1998).
[19]R. M. A. Azzam and N. M. Bashara, *Ellipsometry and Polarized Light* (North-Holland, New York, 1977), p. 354.
[20]C. M. Herzinger, P. G. Snyder, B. Johs, and J. A. Woollam, J. Appl. Phys. **77**, 4 (1995).
[21]F. Gervais, B. Piriou, and D. Billard, Solid State Commun. **17**, 7 (1975).
[22]J. Humlíček and A. Röseler, Thin Solid Films **234**, 1–2 (1993).
[23]M. Albani and P. Bernardi, IEEE Trans. Microwave Theory Techn. **22**, 4 (1974).
[24]A. Taflove and S. C. Hagness, *Computational Electrodynamics: The Finite-Difference Time-Domain Method*, 3rd ed. (Artech House, Norwood, MA, 2005).
[25]K. Joulain, J. Mulet, F. Marquier, R. Carminati, and J. Greffet, Surf. Sci. Rep. **57**, 3 (2005).
[26]A. D. Boardman, *Electromagnetic Surface Modes* (Wiley, Chichester, 1982), p. 776.
[27]V. N. Lyubimov and D. G. Sannikov, Sov. Phys. Solid State **14**, 574 (1972).
[28]B. E. Sernelius, *Surface Modes in Physics* (Wiley - VCH, Berlin, 2001).
[29]J. Le Gall, M. Olivier, and J. Greffet, Phys. Rev. B **55**, 15 (1997).
[30]N. Dahan, A. Niv, G. Biener, Y. Gorodetski, V. Kleiner, and E. Hasman, J. Heat Transfer **130**, 11 (2008).
[31]S. Fan, W. Suh, and J. D. Joannopoulos, J. Opt. Soc. Am. A **20**, 3 (2003).